FULL PAPER

Dalton
www.rsc.org/dalton

Spectral resolution of fluxional organometallics. The observation and FTIR characterization of all-terminal $[Rh_4(CO)_{12}]$

Ayman D. Allian and Marc Garland*

Department of Chemical and Biomolecular Engineering, 4 Engineering Drive 4, National University of Singapore, Singapore 117576. E-mail: chemvg@nus.edu.sg.; Fax: +65-6-779-1936; Tel: +65-6-874-6617

Received 6th January 2005, Accepted 13th April 2005
First published as an Advance Article on the web 16th May 2005

In situ FTIR spectroscopy at 1 cm^{-1} resolution was conducted on n-hexane solutions of the bridged $[Rh_4(CO)_9(\mu\text{-}CO)_3]$ in the interval $T = 268$–288 K and $P_T = 0.1$–7.0 MPa using either helium or carbon monoxide as dissolved gas. Analysis of the spectral data sets was conducted using band-target entropy minimization (BTEM), in order to recover the pure component spectra. A new spectral pattern was recovered with terminal vibrations at 2075, 2069.8, 2044.6 and 2042 cm^{-1}. The new spectrum is consistent with an all-terminal $[Rh_4(CO)_{12}]$ species with a C_{3v} anticube-octahedron structure where 2 different $[Rh(CO)_3]$ moieties exist, although the presence of some T_d structure can not be entirely excluded. The equilibrium between all-terminal $[Rh_4(CO)_{12}]$ and the bridged $[Rh_4(CO)_9(\mu\text{-}CO)_3]$ was determined in the presence of both helium and CO. The equilibrium constant $K_{eq} = [Rh_4(CO)_{12}]/[Rh_4(CO)_9(\mu\text{-}CO)_3]$ at 275 K was *ca.* 0.011 and the determined equilibrium parameters were $\Delta_r G = 12.63 \pm 4.8$ kJ mol^{-1}, $\Delta_r H = -21.45 \pm 2.3$ kJ mol^{-1} and $\Delta_r S = -114.3 \pm 8.35$ J mol^{-1} K^{-1}. The free energy indicates a very small difference between the bridged and terminal geometry, and the lower entropy is consistent with a higher symmetry. This finding helps to address a long-standing issue concerning the existence of various $[M_4(CO)_{12}]$ symmetries. In a more general context, the present study illustrates the considerable utility of quantitative infrared spectroscopy (occurring on a fast vibrational timescale) combined with sophisticated deconvolution techniques in order to resolve systems which have been demonstrated to be fluxional on the NMR timescale.

Introduction

The Group VIII (Co, Rh, Ir) tetranuclear metal carbonyl clusters $[M_4(CO)_{12}]$ have been the subject of intense research for over 40 years. In particular, their structures and fluxional behavior in solution have generated considerable discussion.[1–7] Three primary all-terminal geometries $[M_4(CO)_{12}]$ obeying the 18e-rule for closed polyhedra have been discussed, namely the (1) T_d symmetric cubeoctahedral, (2) the T symmetric icosahedron and (3) the C_{3v} anticubeoctahedron.[5,8,9,10] In addition two bridged species have been discussed, (4) the C_{3v} symmetric icosahedral $[M_4(CO)_9(\mu\text{-}CO)_3]$ and (5) the D_{2d} symmetric $[M_4(CO)_8(\mu\text{-}CO)_4]$. For completeness, it can be mentioned that (6) a triply bridged CO geometry $(CO)_8(\mu_3\text{-}CO)_4]$ has also been suggested as a possible geometry.[4] Fig. 1 provides representations for these structures.

In the case of cobalt, the X-ray crystal structure shows a C_{3v} symmetric icosahedral $[Co_4(CO)_9(\mu\text{-}CO)_3]$.[11–16] In solution, both the normal infrared spectra and the ^{13}CO enriched spectra are consistent with the same geometry.[17,18] In addition, the ^{13}C NMR,[19] ^{17}O NMR[20] and the ^{59}Co NMR[21–24] solution spectra are also consistent with the C_{3v} symmetric icosahedral geometry. The ^{13}CO NMR studies provided clear evidence for cluster fluxional behavior at higher temperatures particularly coalescence at *ca.* 283 K.[10,23,25,26] In the case of the iridium X-ray crystal structure, a complication arises due to the presence of 3 distinct molecules in the unit cell. However, it was concluded that there is essentially T_d symmetric cubeoctahedral $[Ir_4(CO)_{12}]$.[27,28] The T_d symmetry is preserved in solutions as indicated by ^{13}CO NMR[29] and IR spectroscopy.[30]

The rhodium cluster $[Rh_4(CO)_{12}]$ represents a special case due in part to its highly fluxional behavior. The reddish orange $[Rh(CO)_3]_n$ was first reported by Heiber and Lagally,[31] and Chini reported the synthesis and isolation of $[Rh_4(CO)_{12}]$.[32–34] The X-ray structure has been determined on at least 3 occasions, and an idealized C_{3v} symmetric icosahedral $[Rh_4(CO)_9(\mu\text{-}CO)_3]$ has been shown.[14,35,36] In solution, the infrared[18] and the Raman spectra[37] are consistent with the same geometry at room

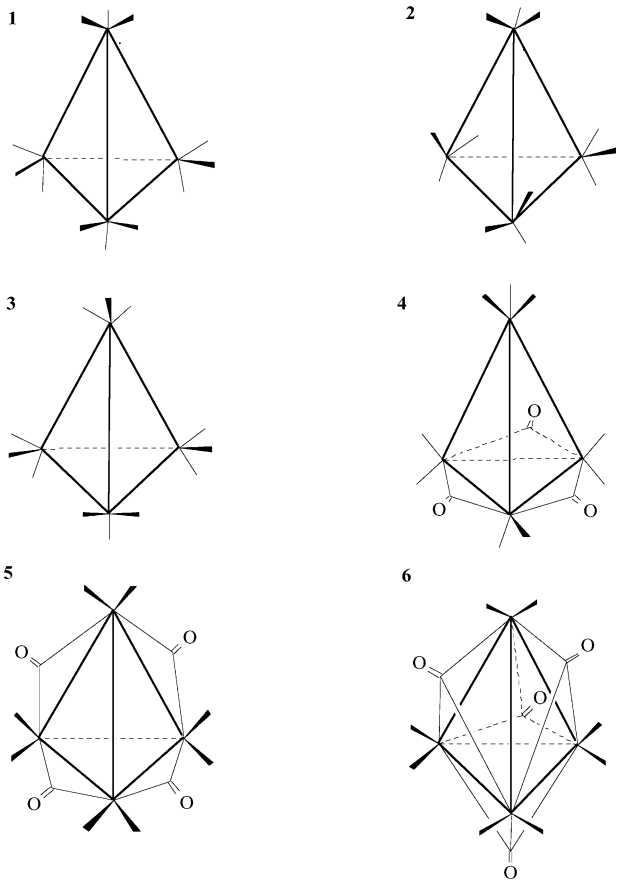

Fig. 1 The proposed structures for $[M_4(CO)_{12}]$: (1) T_d cubeoctahedron; (2) T icosahedron; (3) C_{3v} anticubeoctahedron; (4) C_{3v} icosahedron; (5) D_{2d} with four bridging carbonyls; (6) triply bridged (structures 1–4, 5 and 6 were adapted from ref. 5, 15 and 4 respectively).

DOI: 10.1039/b500044k

temperature. In addition, the ^{13}C NMR[3,10] and ^{103}Rh solution spectra[38] are also consistent with the bridged C_{3v} symmetric icosahedral geometry at least in the vicinity of 213 K. However, at *ca.* 268 K coalescence occurs[3,10,39] indicating equivalence of all CO ligands on the NMR timescale. This suggests the interconversion: bridged C_{3v} ↔ all-terminal ↔ bridged C_{3v}.[1–3,9,10] The possible all-terminal geometries include T_d cubeoctahedron, T icosahedron and C_{3v} anticubeoctahedron. Arguments exist to support the T icosahedron geometry as the lowest energy configuration.[40,41]

Rhodium and rhodium carbonyl complexes in the presence of CO, either in matrices or solution, have yielded numerous mononuclear and polynuclear species. An extensive list is provided in Table 1. The interconversion between $[Rh_4(CO)_{12}]$ and $[Rh_2(CO)_6(\mu\text{-}CO)_2]$ is extremely rapid,[42–44] and the omnipresence of $[Rh_6(CO)_{12}(\mu_3\text{-}CO)_4]$ is consistently observed even under high CO pressure.

In the present contribution, the solution chemistry of $[Rh_4(CO)_{12}]$ is re-investigated under various helium or CO partial pressures in n-hexane as solvent in the interval T = 268–288 K and P_T = 0.1–7.0 MPa using FTIR as the spectroscopic tool and band-target entropy minimization (BTEM) as the signal processing algorithm.[50,51] BTEM has repeatedly shown its ability to retrieve pure component spectra with very weak signal intensities, *i.e.* $[HRh(CO)_4]$.[52] Since infrared spectroscopy has a significantly faster timescale than NMR[4] and since these experiments are conducted above the NMR coalescence temperature, one or more all-terminal geometries should be resolvable, if the superimposed signals can be adequately deconvoluted.

More generally, the problem of fluxionality on the NMR timescale and its resolution on a fast infrared timescale can be illustrated using Scheme 1. Organometallic molecules $[M_xL_n]$ with geometries 1 and 2 exist in equilibrium exchange, where the transition state ‡ separates the two states. If transformation occurs on a NMR timescale, then the signal(s) are broadened and are no longer specific to the individual states involved. In contrast, infrared spectroscopy, occurring on the vibration timescale, can discern the individual states. Thus infrared spectroscopy, coupled with a sophisticated deconvolution technique, holds considerable promise for resolving spectroscopically similar states in fluxional systems.

$$[M_xL_n(1)] \leftrightarrow [M_xL_n]^{\ddagger} \leftrightarrow [M_xL_n(2)]$$

Scheme 1 The transformation of an organometallic $[M_xL_n(1)]$, through a transition state $[M_xL_n]^{\ddagger}$, to another organometallic $[M_xL_n(2)]$ and then back to its original form $[M_xL_n(1)]$. This equilibrated exchange process is typically said to be fluxional if it occurs on the NMR timescale.

Table 1 List of known unsubstituted neutral rhodium carbonyl species relevant to *in situ* spectroscopic studies in matrices and hydrocarbon solutions

Species	Band/cm^{-1}	Ref.
[Rh(CO)]	2012.8, 2008[a]	45
$[Rh(CO)_2]$	2014.6[a]	45
$[Rh(CO)_3]$	2018.4[a]	45
$[Rh(CO)_4]$	2019, 2012[a]	45
$[Rh_2(CO)_6(\mu\text{-}CO)_2]$	2060, 2043, 2038, 1852, 1830[a]	46
	2086, 2061, 1860, 1845[b]	42
	2084, 2060, 1862, 1847[c]	43
	2087, 2062, 1852, 1832[e]	44
	2084.6, 2060.2, 1861.2, 1845.4[c]	This study
$[Rh_4(CO)_9(\mu\text{-}CO)_3]$	2076, 2071, 2045, 1886[b]	42
	2075, 2070, 2045, 1887[c]	43
	2076, 2072, 2045, 1885[d]	44
	2074, 2069, 2043, 1885[c]	47
	2075.2, 2070, 2044.8, 2042.8, 1885.6[c]	This study
$[Rh_6(CO)_{12}(\mu_3\text{-}CO)_4]$	2070, 1793[e]	48
	2077, 2046, 1805[f]	49
	2075.4, 2044.6, 1818.6[c]	This study

[a] Argon matrix. [b] Liquid paraffin–heptane mixture. [c] Hexane. [d] Dodecane. [e] Nujol. [f] Chloroform.

Results

Spectroscopic aspects

Seven isothermal semibatch reactions were conducted. Five were conducted in the presence of CO and two were conducted in the presence of helium. Although the experimental spectral range was 1000–2500 cm^{-1}, large regions contained no identifiable changes, and the spectral data was truncated to the region 1800–2100 cm^{-1}. The 7 semibatch reactions resulted in 475 *in situ* spectra. These were consolidated into one matrix $\mathbf{A}_{475 \times 1501}$.

Singular value decomposition (SVD) and BTEM

In order to extract the pure components, the matrix was deconvoluted *via* BTEM without any preconditioning. Mathematical details of BTEM are available elsewhere.[50,51] The first step in BTEM is the singular value decomposition (SVD) of the observed spectra, $\mathbf{A}_{475 \times 1501}$, in order to obtain the right singular V^T matrix whose row vectors contain untangled and abstract information on the pure component spectra. Indeed, inspection of the V^T vectors reveals the characteristic features of the pure components spectra present in solution as shown in Fig. 2, where some particularly noteworthy spectral features have been marked.

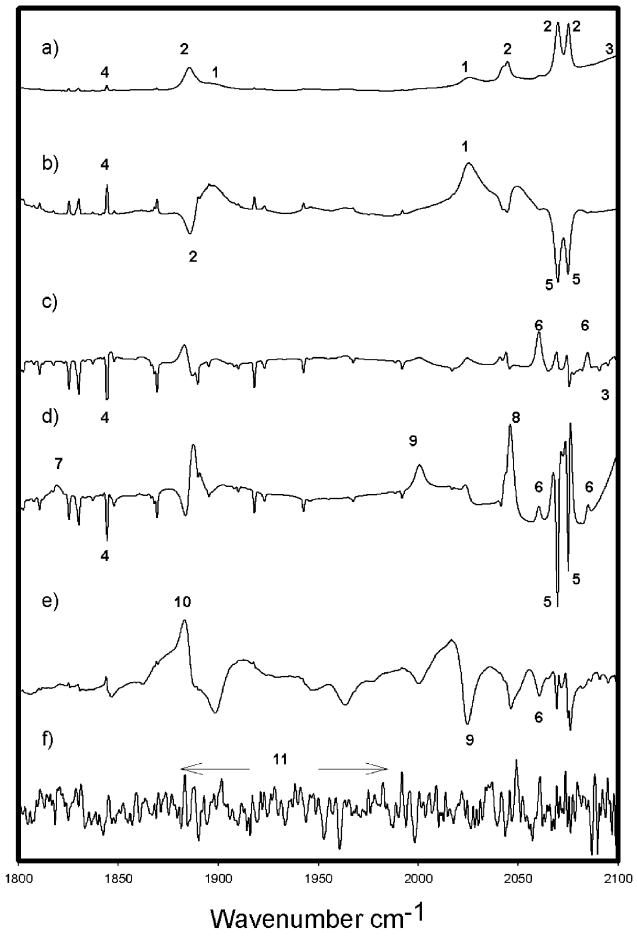

Fig. 2 Several right singular vectors (V^T) from the SVD of the experimental data: a) 1st vector, b) 3rd vector, c) 6th vector, d) 7th vector, e) 12th vector, f) 70th vector.

The BTEM algorithm was used to target individual spectral features of interest in V^T vectors, and subsequently reconstruct pure component spectra one-at-a-time. A list of the targeted spectral features from Fig. 2 used for the BTEM calculations and the resultant pure components obtained are shown in Table 2.

Table 2 List of the bands used for BTEM calculations and resultant pure components

Spectral marker	Marked spectral positions/cm^{-1}	Recovered species	V^T vector where marker is first indicated in Fig. 2	Singular value associated with V^T vector
1	2025.4, 1896	Hexane-solvent	1	640.07
2	2075.2, 2070, 2044.8, 1885.6	$[Rh_4(CO)_9(\mu\text{-}CO)_3]$	1	640.07
3	2096	CO dissolved gas	1	640.07
4	1844.2	Moisture	1	640.07
5	2075, 2069.8	Species X	3	29.119
6	2084.6, 2060.2	$[Rh_2(CO)_6(\mu\text{-}CO)_2]$	6	1.8009
7	1818	$[Rh_6(CO)_{12}(\mu_3\text{-}CO)_4]$	7	1.0877
8	2046	$[Ni(CO)_4]$	7	1.0877
9	2023.6	$[Fe(CO)_5]$	7	1.0877
10	1883	Failed attempts	12	0.4840
11	Mostly white noise		70	0.01487

It is useful to mention that SVD orders the vectors according to their associated singular values, which represent their contribution to the total variance in the observations. Thus, features associated with major components having high concentrations appear in the initial vectors with large singular values, while the features associated with minor components usually emerge in the latter vectors with smaller singular values. The ratio of component signal to random noise is largest in the first vector and decreases with subsequent vectors. The 70th right singular vector is predominantly white noise.

The pure component spectra of all the metal carbonyls observed in this study are shown in Fig. 3. The pure component spectra, arising from the rhodium carbonyls $[Rh_4(CO)_9(\mu\text{-}CO)_3]$ and $[Rh_6(CO)_{16}]$, possess very high signal to noise ratios. The pure component spectra from $[Rh_2(CO)_6(\mu\text{-}CO)_2]$ and the species X, have slightly elevated noise levels. The pure component spectra from $[Ni(CO)_4]$ and $[Fe(CO)_5]$, which are at trace concentrations, have relatively high noise levels. The wavenumbers for the rhodium carbonyls mentioned above and determined in this study are presented in Table 1. It can be noted, that the use of higher resolution has allowed the observation of the splitting of the broad band of the bridged $[Rh_4(CO)_9(\mu\text{-}CO)_3]$ at *ca.* 2043 cm^{-1} into a sharp band at 2044.8 cm^{-1} and a shoulder at 2042.8 cm^{-1}. This result is in agreement with the observed spectra of $[Rh_4(CO)_9(\mu\text{-}CO)_3]$ made by Bor.[18] The observed wavenumbers for $[Ni(CO)_4]$ and $[Fe(CO)_5]$ were 2046 and 2023.6, 2000.4 cm^{-1} respectively, consistent with the literature values.[53,54] The impurity $[Fe(CO)_5]$ is frequently present in commercial CO gas stored in steel cylinders, but the present *in situ* study is the first in which this group has been able to identify the presence of $[Ni(CO)_4]$. In addition, with higher resolution, a third peak for $[Rh_6(CO)_{16}]$ at 2045.6 cm^{-1} is more clearly seen in this study, compared to previous studies by this group.[55] The spectrum of $[Rh_6(CO)_{16}]$ is in agreement with the one obtained by Beck[56] and Weber[49] and consistent with the molecular geometry T_d.[57] No further pure component metal carbonyl spectra could be readily obtained.

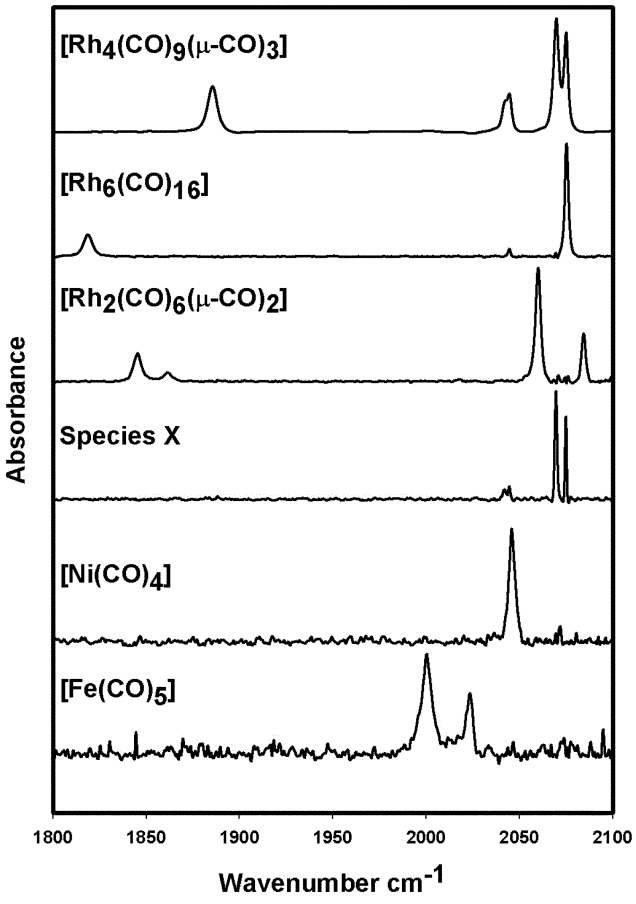

Fig. 3 Pure component spectra obtained from BTEM analysis.

Signal recovery in this study was high. The signal contribution of each pure component to the total observed signal is shown in Table 3. The organometallic species contribute *ca.* 25% of the signal in the 5 CO containing experiments, and *ca.* 40% of the signal in the 2 He containing experiments. The sum total of all signals recovered is very close to 100% in both the CO and He experiments.

Normalized concentrations

Each of the 7 semibatch reactions consisted of 2 additions of $[Rh_4(CO)_9(\mu\text{-}CO)_3]$ to the system, and many perturbations in CO or helium (see Experimental section). The first addition of $[Rh_4(CO)_9(\mu\text{-}CO)_3]$ corresponds to the pressure interval 0.1–2.0 MPa and the second addition of $[Rh_4(CO)_9(\mu\text{-}CO)_3]$ corresponds to the pressure interval 3.0–7.0 MPa. Fig. 4 provides the normalized concentrations of all the metal carbonyl species for these 7 semibatch experiments consisting of 475 spectral

Table 3 Percentage of reconstructed integrated absorbance of each component compared to the total original experimental data

Components	Signal ratio (%)	
	CO set	He set
Hexane	35.64	57.41
$[Rh_4(CO)_9(\mu\text{-}CO)_3]$	22.89	37.74
Dissolved CO	39.95	[a]
Moisture	1.002	2.134
Species X	0.736	1.77
$[Rh_2(CO)_6(\mu\text{-}CO)_2]$	0.710	[a]
$[Rh_6(CO)_{16}]$	0.375	0.130
$[Ni(CO)_4]$	0.371	[a]
$[Fe(CO)_5]$	0.123	[a]
Total	101.7	99.23

[a] Signal undetected.

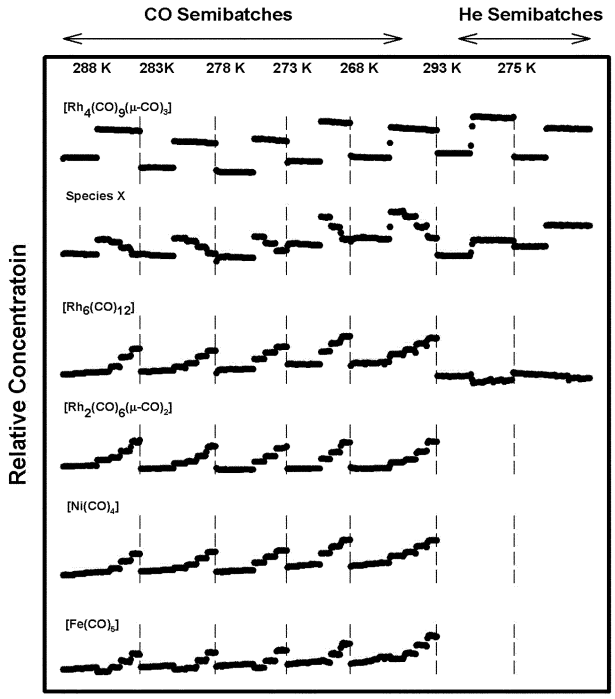

Fig. 4 The normalized metal carbonyl concentrations provided by BTEM analysis for the 7 semibatch reactions. Note that the mean concentrations of the species vary over many orders of magnitude, therefore, one-to-one comparison of the individual scales in the figure is not possible.

measurements. Since the pure component spectra obtained from BTEM in Fig. 3 are all of unit height, the calculated concentrations shown in Fig. 4 are relative and not properly scaled at this point in the analysis.

The CO experiments show that (1) the concentrations of X are fixed ratios of the $[Rh_4(CO)_9(\mu\text{-}CO)_3]$ concentrations for the first perturbation of $[Rh_4(CO)_9(\mu\text{-}CO)_3]$ up to 2.0 MPa CO but slowly decrease during the second perturbation of $[Rh_4(CO)_9(\mu\text{-}CO)_3]$ up to 7.0 MPa CO, (2) the omnipresent but not equilibrated $[Rh_6(CO)_{16}]$ exists in all experiments, and generally increases with increasing CO pressure (addition of more impurities promotes formation), (3) the equilibrated dinuclear complex $[Rh_2(CO)_6(\mu\text{-}CO)_2]$ increases as a function of CO pressure as anticipated and (4) the impurities $[Ni(CO)_4]$ and $[Fe(CO)_5]$ increase with increasing CO pressure.

The helium experiments show that (1) the concentrations of X are fixed ratio's of the $[Rh_4(CO)_9(\mu\text{-}CO)_3]$ concentrations even under variable pressure, (2) the concentration of $[Rh_6(CO)_{16}]$ is non-zero and shows little variation with increasing pressure during each semi-batch run and (3) the dinuclear complex $[Rh_2(CO)_6(\mu\text{-}CO)_2]$ is not formed since no excess CO is present. This last observation is consistent with Whyman's work with $[Rh_4(CO)_9(\mu\text{-}CO)_3]$ under nitrogen.[42]

Preliminary interpretation of the new experimental spectrum

As seen from Fig. 3, the species X has no bridging CO. This spectrum was obtained using 70 basis vectors V^T. In order to check whether any serious signal artifacts were introduced into the spectral reconstruction, a validation/uniqueness test in the form of target transform factor analysis (TTFA)[58] was carried out. In this analysis, the BTEM reconstruction of X is projected onto the reduced vector-space formed from the first 25 V^T vectors. If the resulting vector is very similar to the tested vector, then the reconstructed spectrum probably does not contain any serious artifacts. This is indeed the case as seen in Fig. 5. Furthermore, an expanded view of the terminal region is provided in Fig. 5 where the spectrum of $[Rh_4(CO)_9(\mu\text{-}CO)_3]$

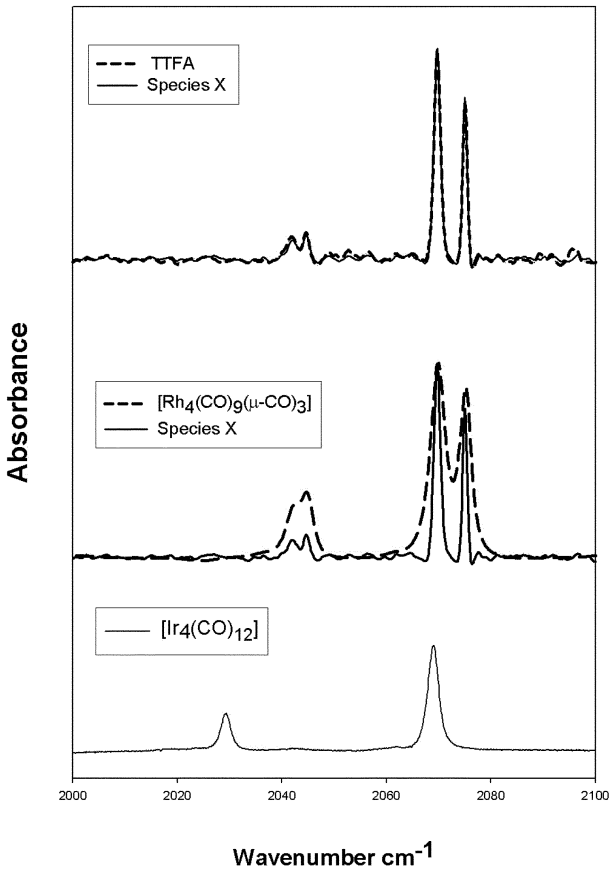

Fig. 5 Validation/uniqueness test using TTFA (above). The spectrum of species X superimposed on that of $[Rh_4(CO)_9(\mu\text{-}CO)_3]$ in the terminal CO region (middle). Additional comparison to the T_d symmetry of $[Ir_4(CO)_{12}]$ (below).

is superimposed. The 4 bands of X, at 2075, 2069.2, 2044.6, 2042 cm^{-1} are virtually coincident with the terminal bands of $[Rh_4(CO)_9(\mu\text{-}CO)_3]$ but much narrower. In addition, the species X appears to be two super-imposed patterns similar to the all-terminal $[Ir_4(CO)_{12}]$. The latter possesses T_d symmetry where each of the $[Ir(CO)_3]$ moieties are equivalent and have two vibrational bands.[30] Therefore, the new spectrum suggests that there are two $[Rh(CO)_3]$ groups present with different local environments.

The normalized concentration profiles in Fig. 4, particularly those under helium and those under CO up to and including 2.0 MPa, indicate that the concentration of the new species X is a fixed ratio compared to $[Rh_4(CO)_9(\mu\text{-}CO)_3]$ at any temperature T. This concentration dependence is consistent with an elemental stoichiometry for the species X identical to $[Rh_4(CO)_{12}]$. We propose that the species X is in fact, at least 1 isomer of the all-terminal $[Rh_4(CO)_{12}]$. The BTEM recovered spectrum could represent (A) just one isomer of $[Rh_4(CO)_{12}]$ possessing two different $[Rh(CO)_3]$ moieties or (B) more than one isomer of all-terminal $[Rh_4(CO)_{12}]$.

Real concentrations and equilibria

The data for the CO series of experiments were regressed to obtain the absolute (rather than normed) absorptivities for the 4 rhodium carbonyl clusters, namely, $[Rh_4(CO)_9(\mu\text{-}CO)_3]$, all-terminal $[Rh_4(CO)_{12}]$, $[Rh_2(CO)_6(\mu\text{-}CO)_2]$ and $[Rh_6(CO)_{12}(\mu_3\text{-}CO)_4]$. The mass balances for rhodium in each semibatch run, and each perturbation within the run, were used to constrain the numerical solutions. Details of similar optimization methods to properly scale absorptivities can be found elsewhere.[58]

The maximal absorptivities for $[Rh_4(CO)_9(\mu\text{-}CO)_3]$, $[Rh_4(CO)_{12}]$, $[Rh_2(CO)_6(\mu\text{-}CO)_2]$ and $[Rh_6(CO)_{12}(\mu_3\text{-}CO)_4]$ were; 2.82×10^4 l mol^{-1} cm^{-1} (2070 cm^{-1}), 2.85×10^5 l mol^{-1} cm^{-1}

(2069.8 cm^{-1}), 2.72×10^4 l mol^{-1} cm^{-1} (2060.2 cm^{-1}) and 1.34×10^5 l mol^{-1} cm^{-1} (2075.4 cm^{-1}) respectively. The absolute values for the absorptivities of $[Rh_4(CO)_9(\mu\text{-}CO)_3]$ and $[Rh_2(CO)_6(\mu\text{-}CO)_2]$ determined in this study are only marginally higher (*ca.* 10%) than those previously determined,[43,59] and this can be traced to the slightly higher resolution used in this study, as well as the more accurate mass balances.

An independent calibration for $[Rh_6(CO)_{12}(\mu_3\text{-}CO)_4]$ in n-hexane proved to be very difficult to obtain due to its extreme low solubility in hexane, but a minimum value of $(4.1 \pm 0.98) \times 10^4$ l mol^{-1} cm^{-1} (2075.4 cm^{-1}) is certain. In addition the pure component spectra of $[Rh_6(CO)_{12}(\mu_3\text{-}CO)_4]$ obtained confirmed the presence of the third peak at 2045.6 cm^{-1}.

Integrating the properly scaled absorptivities of $[Rh_4(CO)_9(\mu\text{-}CO)_3]$ and all-terminal $[Rh_4(CO)_{12}]$ over the data channels used (1501 channels from 1800–2100 cm^{-1}), provided values of 1.8×10^6 l channel mol^{-1} cm^{-1} and 3.7×10^6 l channel mol^{-1} cm^{-1} respectively. Assuming that similar CO force constants are involved, the determined properly scaled absorptivity for $[Rh_4(CO)_{12}]$ cannot be seriously in error.

The maximum mole fractions for $[Rh_4(CO)_9(\mu\text{-}CO)_3]$, $[Rh_4(CO)_{12}]$, $[Rh_2(CO)_6(\mu\text{-}CO)_2]$ and $[Rh_6(CO)_{12}(\mu_3\text{-}CO)_4]$ observed in the entire experimental study were; 6×10^{-5}, 7.5×10^{-7}, 5.5×10^{-7} and 6.5×10^{-7} respectively.

The primary rhodium carbonyl cluster equilibrium present in this study is shown in eqn. (1).

$$K_{eq1} = \frac{[Rh_4(CO)_{12}]}{[Rh_4(CO)_9(\mu\text{-}CO)_3]} \quad (1)$$

The calculated equilibrium constants are shown in Fig. 6.

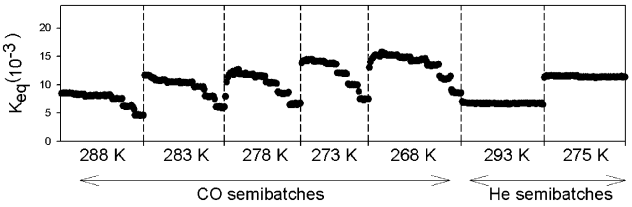

Fig. 6 The calculated equilibrium constants for $[Rh_4(CO)_{12}]$.

The helium data sets as well as the CO data sets below 3.0 MPa provided consistent equilibrium constants. The reason for the variable K_{eq} at $P > 3.0$ MPa is at the moment not entirely clear but may be due to significantly changing the bulk dielectric constant of the liquid phase when more than *ca.* 3 mole percent of dissolved CO is present. The lower pressure data was regressed for $K_{eq}(T)$. A Van't Hoff plot is provided in Fig. 7.

Concluding remarks on the possible role of impurities

In the present results, the mean concentrations of the new species $[Rh_4(CO)_{12}]$ was estimated as *ca.* 0.6×10^{-6} mole fraction. Since impurities are always present in chemical systems, and since the new species exists at such low concentrations, the possibility of misinterpretation of the results should be addressed. The possibility that the new species represents one or more impurities can be excluded with considerable certainty, using the following arguments. First, if the spectrum X was associated with an impurity in the starting material *i.e.* an $[Rh_x(CO)_yL]$ complex present in the polycrystalline $[Rh_3(CO)_9(\mu\text{-}CO)_3]$, then its concentration would not be expected to be a function of temperature, and/or its concentration would be influenced during the 0–3.0 MPa partial pressure CO experiments, and finally the observed terminal CO vibrations should be broad/broader due to lower symmetry (*infra vida*). Secondly, if a species $[Rh_x(CO)_yL]$ were produced *in situ* from coordination/reaction of a fixed amount of an impurity L (*i.e.* from the solvent) with $[Rh_4(CO)_{12}]$, then the concentration of $[Rh_x(CO)_yL]$ would be influenced during the 0–3.0 MPa partial pressure CO experiments, and as well, the observed terminal CO vibrations should be broad/broader. Third, if a species $[Rh_x(CO)_yL]$ were produced *in situ* from coordination/reaction of a variable amount of an impurity L (*i.e.* from introduced CO) with $[Rh_4(CO)_{12}]$, then the concentration of $[Rh_x(CO)_yL]$ would be influenced during the 0–3.0 MPa partial pressure CO experiments, the observed terminal CO vibrations should be broad/broader, and $[Rh_x(CO)_yL]$ should not be identifiable in the helium series of experiments. Since such correlations/observations are not present in the experiments performed, the probability that one or more $[Rh_x(CO)_yL]$ complexes has lead to misinterpretation of the results seems extremely remote.

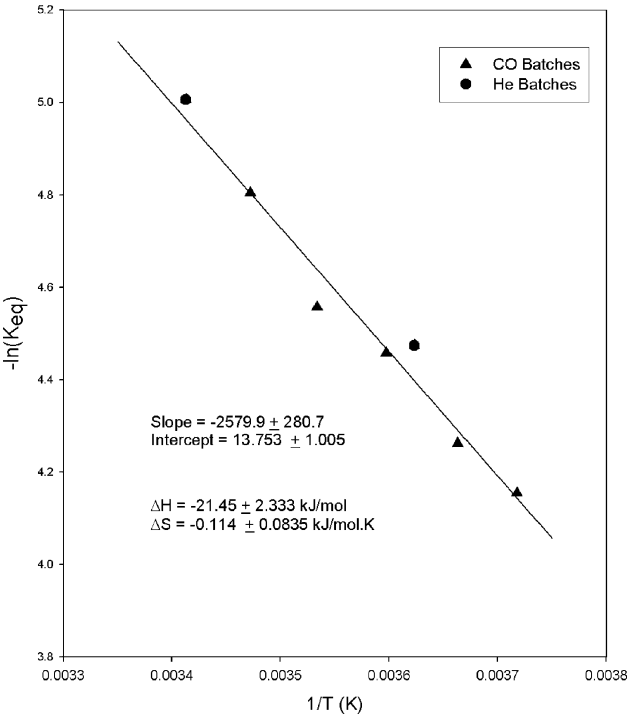

Fig. 7 Estimation of thermodynamic parameters based on the Van't Hoff equation.

Discussion

In recent years, indications for the existence of observable quantities of all-terminal $[Rh_4(CO)_{12}]$ have been obtained during *in situ* infrared spectroscopic studies of the unmodified rhodium catalyzed hydroformylation made with 4 cm^{-1} resolution.[51,52] The narrow bands at *ca.* 2068 and 2076 cm^{-1} were observed, but the presence of bands in the region of 2040 cm^{-1} could not be conclusively substantiated. In the present study, far more spectra have been measured, under non-catalytic conditions, with higher resolution 1 cm^{-1}, and under a much wider range of CO/He partial pressures. Similar narrow bands are again deconvoluted, but more importantly, 2 bands at 2044.6 and 2042 cm^{-1} have been resolved. The thermodynamic data confirms the stoichiometry $[Rh_4(CO)_{12}]$, and the free energy of reaction indicates a structure only 12 kJ mol^{-1} higher than $[Rh_4(CO)_9(\mu\text{-}CO)_3]$.

The spectra of all-terminal $[Rh_4(CO)_{12}]$ and variety of structures

As stated previously in the Results section, the present spectrum of $[Rh_4(CO)_{12}]$ arises either from (A) one isomer possessing two different $[Rh(CO)_3]$ groups or (B) more than one isomer of an all-terminal $[Rh_4(CO)_{12}]$ molecule. The line shapes are considerably narrower than usual for rhodium carbonyl species. The deconvoluted spectra indicate line widths at half height of *ca.* 2 cm^{-1} for $[Rh_4(CO)_{12}]$ compared to *ca.* 5 cm^{-1} for $[Rh_4(CO)_9(\mu\text{-}CO)_3]$ in the terminal CO region. This is consistent with the fact that higher molecular symmetry leads to more localized energy levels. This tendency is readily apparent in a

variety of systems including (i) $[Mo(CO)_6]$ and $[Mo(CO)_5PPh_3]$,[60] (ii) $[Mn_2(CO)_{10}]$ and $[Mn_2(CO)_9]$[61] and (iii) $[\{(C_6H_{11})_3P\}_2Mo(CO)_4]$ and *trans*$[\{(Pr^iO)_3P\}_2Mo(CO)_4]$ where the "irregular packing of the PrO fragment" in the latter significantly broadened the IR bands.[62]

If case (A) is occurring, then there is one isomer possessing two different $[Rh(CO)_3]$ groups. This excludes T_d symmetric $[Rh_4(CO)_{12}]$ by itself since only 2 bands will arise. The *T*-icosahedron is believed to have the lowest energy of the all the suggested $[M_4(CO)_{12}]$ terminal structures[41] but this geometry is not consistent with 4 observable bands. The C_{3v} anticuboctahedron symmetry was suggested by Johnson, as the most appropriate intermediate that can explain the total coalescence of the NMR signal at $T = -5$ K, and has two different $[Rh(CO)_3]$ groups, *i.e.* those on the basal plane, α, and the apical group, β, as shown in Fig. 8. This would be consistent with four observed bands.

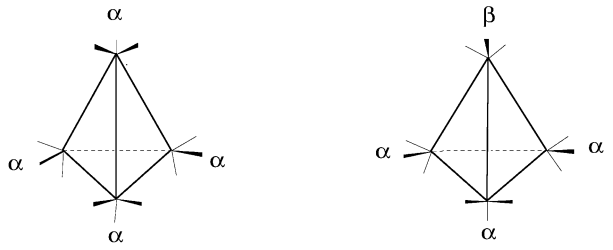

Fig. 8 The two possible geometrical isomers. In the T_d symmetry all $[Rh(CO)_3]$ moieties are similar (α). In contrast, the C_{3v} symmetry's apical $[Rh(CO)_3]$ has a different local environment (β).

In case (B) the new spectrum arises from the simultaneous presence of more than one $[Rh_4(CO)_{12}]$ cluster. For example, one possibility is the simultaneous existence of C_{3v} symmetric $[Rh_4(CO)_{12}]$ (major isomer) and some T_d symmetric $[Rh_4(CO)_{12}]$ (minor isomer). Both have a common $[Rh(CO)_3]$ local symmetry/environment, α, as shown in Fig. 8. Since the integrated areas under the respective bands (*i.e.* 2075 : 2069.2 and 2044.6 : 2042 cm^{-1}) are not exactly 1 : 3 as anticipated if only the C_{3v} isomer were present, the coexistence of some T_d isomer should not be ruled out. It is worth mentioning that a mixture of C_{3v} and T_d will still give rise to 4 observable bands due to superpositions of the signals due to the α groups. It can be noted that the existence of 2 energetically similar clusters is consistent with remarks by Farrugia[63] that "carbon monoxide may bind to ensembles of metal atoms in energetically similar, but geometrically distinct modes".

Expressed in somewhat different form, the BTEM reconstructed spectrum is not conclusive enough by itself to differentiate between the presence of 1 isomer of $[Rh_4(CO)_{12}]$ or the simultaneous presence of 2 isomers of $[Rh_4(CO)_{12}]$. Indeed, the BTEM recovered spectrum could arise if almost-exact collinearity of 2 concentration profiles occurs. NMR data[3,10] confirms that inter-conversion of $[Rh_4(CO)_9(\mu\text{-}CO)_3]$ and $[Rh_4(CO)_{12}]$ isomers is occurring on a fast timescale (*ca.* 10^{-3} s), and the present thermodynamic results confirm that the terminal isomer(s) have only marginally higher free energy. Therefore, given the small temperature interval used, little concentration variation might occur between 2 co-existing isomers and an inseparable superposition of spectra would result.

Although not complete, the identification of all-terminal $[Rh_4(CO)_{12}]$ provides some new information on the fluxional system Scheme 2. Muetterties indicated that the transition state $[Rh_4(CO)_{12}]^{\ddagger}$ has a free energy 56 kJ mol^{-1} greater than $[Rh_4(CO)_9(\mu\text{-}CO)_3]$.[4] The present thermodynamic data indicates that the species $[Rh_4(CO)_{12}]$ has a free energy 12 kJ mol^{-1} greater than $[Rh_4(CO)_9(\mu\text{-}CO)_3]$ or *ca.* 44 kJ mol^{-1} lower than $[Rh_4(CO)_{12}]^{\ddagger}$.

$$[Rh_4(CO)_9(\mu\text{-}CO)_3] \leftrightarrow [Rh_4(CO)_{12}]^{\ddagger} \leftrightarrow [Rh_4(CO)_{12}]$$

Scheme 2 The transformation of the organometallic cluster $[Rh_4(CO)_9(\mu\text{-}CO)_3]$, through one or possibly more transition states $[Rh_4(CO)_{12}]^{\ddagger}$, to $[Rh_4(CO)_{12}]$. This equilibrated exchange process is known to be fluxional on the NMR timescale at *ca.* 298 K. The all-terminal state $[Rh_4(CO)_{12}]$ was resolved by infrared spectroscopy at *ca.* 298 K.

Bulk physico-chemical effects on equilibria

The helium experiments clearly showed that there is no observable total pressure effect on the $[Rh_4(CO)_9(\mu\text{-}CO)_3]$ and $[Rh_4(CO)_{12}]$ equilibrium, and the low pressure CO experiments provide consistent values for the equilibrium constant. However, the high CO partial pressures indicate a decreasing value for K_{eq} as a function of P_{CO}, thus, CO concentration in solution. This effect appears to be associated with a change in a bulk solution physico-chemical property.

Non-polar hexane has a zero dipole moment,[64] and dissolution of atomic helium is not expected to change the bulk dielectric constant since it also has a zero dipole moment.[64] However, the dissolution of CO, with a non-zero dipole moment of 0.1,[65] will increase the bulk solution dielectric constant in a non-negligible manner. In addition, the highly symmetric species $[Rh_4(CO)_{12}]$ should have a vanishingly small overall dipole moment whereas the same cannot be said of $[Rh_4(CO)_9(\mu\text{-}CO)_3]$. Taken together, the above physico-chemical issues argue for a decreasing K_{eq1} with increasing CO concentration. As the solution polarity increases, the least polarized molecule is less favored thermodynamically. This finding raises issues about the importance of bulk physico-chemical properties on organometallic transformations but at the same time, the general lack of such solution property information.

$[Rh_2(CO)_6(\mu\text{-}CO)_2]$. In n-hexane solution, $[Rh_4(CO)_9(\mu\text{-}CO)_3]$ is rapidly converted to $[Rh_2(CO)_6(\mu\text{-}CO)_2]$ according to eqn. (2).

$$[Rh_4(CO)_9(\mu\text{-}CO)_3] + 4CO \leftrightarrow 2[Rh_2(CO)_6(\mu\text{-}CO)_2] \quad (2)$$

The equilibrium constant can be written as shown in eqn. (3).

$$K_{eq2} = \frac{[Rh_2(CO)_6(\mu\text{-}CO_2)^2]}{[Rh_4(CO)_9(\mu\text{-}CO)_3][CO]^4} \quad (3)$$

Under the CO partial pressures used in this study, the maximum conversion observed in this study was only *ca.* 0.4%. The equilibrium between $[Rh_4(CO)_9(\mu\text{-}CO)_3]$ and $[Rh_2(CO)_6(\mu\text{-}CO)_2]$ was also obtained. At low CO pressures, the conversion is too small to provide meaningful values of K_{eq}. At pressures of *ca.* 50–70 bar CO, consistent K_{eq} of *ca.* $(5.21 \pm 2) \times 10^{-3}$ are obtained. The present value of K_{eq2} is reasonably consistent with the literature value provided by Oldani and Bor, and obtained from data in the pressure range of 100–200 bar.[43]

Further spectroscopic signal issues

The presence of an observable triply bridged species $[M_4(CO)_8(\mu_3\text{-}CO)_4]$ is not supported by the present data. A triply bridged CO on a neutral rhodium cluster should give rise to a spectral feature at *ca.* 1820 cm^{-1}, as is the case for $[Rh_6(CO)_{12}(\mu_3\text{-}CO)_4]$. No new unaccountable spectral features in the region 1800–1840 cm^{-1} were seen in the right singular vectors.

Given the well known fluxionality of rhodium carbonyl clusters, and the labile inter-conversion of rhodium carbonyl species, the possible existence of an all-terminal dinuclear rhodium carbonyl $[Rh_2(CO)_8]$ must be considered. This is particularly true in light of the reported coexistence of both the bridged and terminal dimers of the phosphite substituted $[Rh_2(CO)_6\{P(OPh_3)\}_2]$ and $[Rh_2(CO)_7\{P(OPh_3)\}]$.[66] Also, the analogous cobalt chemistry is well documented by the spectroscopic identification of $[Co_2(CO)_8]$ equilibrated in solutions of

$[Co_2(CO)_6(\mu\text{-}CO)_2]$/aliphatic hydrocarbon.[67–69] By comparison with $[HRh(CO)_4]$[52] and $[RCORh(CO)_4]$,[70] a totally symmetric vibration in the region of *ca.* 2110–2130 cm^{-1} may exist due to the local symmetry of the moiety $[Rh(CO)_4]$ in $[Rh_2(CO)_8]$. Extensive analysis of the right singular vectors did not reveal any new spectral features. Since there are many reasons to presume the simultaneous co-existence of $[Rh_2(CO)_8]$ with $[Rh_2(CO)_6(\mu\text{-}CO)_2]$, the present results suggest that its concentration is simply too low for detection. Broadly speaking, if the K_{eq} for the latter species is similar to the observed K_{eq1} between the tetranuclear unbridged dimer and the bridged form, then, only parts-per-billion of the unbridged (1% of the bridged) are expected in solution.

The vibrational signals of the bridged carbonyls in neutral rhodium species occur in the interval of *ca.* 1840–1900 cm^{-1}. The lower wavenumber region is associated with $[Rh_2(CO)_6(\mu\text{-}CO)_2]$ while the higher wavenumber region is associated with higher nuclearity species. As indicated by the SVD results shown in Fig. 2, there was a rather clear indication that more than one spectral feature is embedded in the higher wavenumber bridging CO region of the present experimental data. The most prominent feature is the band at 1885 cm^{-1}, which arises from $[Rh_4(CO)_9(\mu\text{-}CO)_3]$, but a very symmetric feature is also apparent at *ca.* 1883 cm^{-1} when the observations are untangled (see the 12th V^T vector). This feature is only really apparent in the V^T vectors greater than *ca.* 10. This suggests a very low mean concentration.

Repeated attempts to reconstruct the whole spectrum associated with 1883 cm^{-1} using BTEM failed. Reconstructed spectra containing the signal at 1883 cm^{-1} where obtained, however, the spectra were clearly super-positions of more than one species. This is evidenced by features associated with n-hexane as well as other known species. Restricting this discussion to coordinately saturated tetranuclear clusters, the species $[Rh_4(CO)_8(\mu\text{-}CO)_4]$, $[Rh_4(CO)_8(solvent)(\mu\text{-}CO)_3]$,[71] $[Rh_4(CO)_{10}(\mu\text{-}CO)_3]$ and $[Rh_4(CO)_{12}(\mu\text{-}CO)_2]$ are potential candidates. The last two structures would be analogues to the postulated structures $[Co_4(CO)_{10}(\mu\text{-}CO)_3]$ and $[Co_4(CO)_{12}(\mu\text{-}CO)_2]$ discussed at length by Bor.[72]

Impurities

The relative concentration profiles shown in Fig. 4 indicate that the concentrations of $[Ni(CO)_4]$ and $[Fe(CO)_5]$ are zero in the helium experiments and step-wise increasing with CO perturbations. The observed trends are consistent with the known problems associated with commercial grade CO stored in stainless steel cylinders. Although an additional deoxy/zeolite gas purification system was used (see Experimental section for further details), minute quantities of these carbonyl impurities enter the reaction system. By visual inspection, neither $[Ni(CO)_4]$ nor $[Fe(CO)_5]$ can be seen in the experimental spectra. Only after SVD is performed (see Fig. 2) can these species be detected, and only after BTEM is it possible to confirm their identities. The SVD results (Fig 2), BTEM results (Fig 3) and the numerical results (Table 2), namely (1) the presence of spectral features in $V^T = 6, 7$, (2) the relatively low signal to noise ratio of *ca.* 15 : 1 and 10 : 1, and (3) the very small integrated signal intensities confirm the very low concentrations present.

In Fig 4, the concentrations of $[Rh_6(CO)_{16}]$ remained essentially constant in the helium experiments, and gradually increased during the CO semibatch experiments. At the temperatures and conditions used in this study, $[Rh_6(CO)_{16}]$ is not equilibrated with $[Rh_4(CO)_9(\mu\text{-}CO)_3]$. Indeed, if it were in equilibrium exchange, the concentrations of $[Rh_6(CO)_{16}]$ would decrease rather than increase with increasing CO. The observed trends are consistent with the typical ultra-high purity of commercial helium compared to the typical purity of commercial CO (see Experimental section for further details). Although an additional deoxy/zeolite purification system was used for gases prior to use, minute quantities of impurities enter the reaction system. In any typical experiment at *ca.* 50 bar pressure, 5×10^{-5} mol $[Rh_4(CO)_9(\mu\text{-}CO)_3]$, 2 mol of solvent and *ca.* 0.2 mol of gas were present. The step-wise increase in $[Rh_6(CO)_{16}]$ concentrations is undoubtedly associated with the introduction of trace gas-phase impurities and the subsequent degradation of $[Rh_4(CO)_9(\mu\text{-}CO)_3]$.

Resolution, BTEM and time-scales

This study is the first in which 1 cm^{-1} resolution and BTEM have been combined for an organometallic study. The increased resolution permitted more exact deconvolution of the species present using BTEM. For example, this is the first study in which $[Ni(CO)_4]$ was successfully deconvoluted in the presence of rhodium carbonyls. The extreme overlap between the band at 2046 cm^{-1} for $[Ni(CO)_4]$ and that at 2044 cm^{-1} for $[Rh_4(CO)_{12}]$ is very problematic, especially when the ratio of signal intensity in that region is of the order of 10%. Also, the resulting BTEM spectral estimates are, on average, a little narrower. This permits total signal recovery very close to 100% as shown in Table 3.

One possible drawback for the use of high resolution is the observation of rotational modes for dissolved CO which can complicate deconvolution. These modes can be seen in Fig. 2 at *ca.* 2096 cm^{-1}. At lower resolution, these rotational modes are not apparent and BTEM deconvolution is more readily achieved.

Perhaps the most important broad implication of the present study concerns the combined use of faster-than-NMR spectroscopies and BTEM to resolve NMR fluxional systems.

Conclusion

High resolution infrared spectroscopy was combined with the BTEM deconvolution technique in order to obtain the pure component spectrum of the all-terminal cluster $[Rh_4(CO)_{12}]$. This was achieved in spite of the fact that there was only *ca.* 1% conversion of the starting cluster $[Rh_4(CO)_9(\mu\text{-}CO)_3]$, and that the terminal vibrations of both species are very similar. The deconvolution was accomplished in the temperature regime where the system is fluxional on the NMR timescale. The quantitative high pressure infrared measurements confirmed the stoichiometry and provided the free energy, enthalpy and entropy of reaction. The present results have straightforward general implications for the analysis of fluxional systems, namely, a fast timescale spectroscopy (infrared) combined with deconvolution can resolve spectroscopically complex systems.

Experimental

General information

All solution preparations and transfers were carried out under a purified argon (99.9995%, Saxol, Singapore) atmosphere using standard Schlenk techniques.[73] The argon was further purified before use by passing it through a deoxy and zeolite column. Purified carbon monoxide (Research grade, 99.97%, Linde, Singapore) and helium (99.9995%, Saxol, Singapore) were also further purified through a deoxy and zeolite columns before they were used in the experiments. Purified nitrogen (99.9995%, Saxol, Singapore) was used to purge the Perkin-Elmer FT-IR spectrometer system.

$[Rh_4(CO)_9(CO)_3]$ (98%) was purchased from Strem Chemicals (Newburyport, MA, USA) and was used as obtained. The Puriss quality n-hexane (99.6%, Fluka AG) was distilled from sodium–potassium under argon for *ca.* 5 hours to remove the trace water and oxygen.

Apparatus

In situ studies were performed in a 1.5 l stainless steel (SS316) autoclave (P_{max} = 22.5 MPa, Buchi-Uster, Switzerland) which

was connected to a high pressure infrared cell. The autoclave was equipped with a packed magnetic stirrer with six-bladed turbines in both the gas and liquid phases (Autoclave Engineers, Erie, PA) and had a mantle for heating/cooling. The liquid-phase reaction mixtures were circulated from the autoclave to-and-from the high pressure IR cell with a high membrane pump (Model DMK 30, Orlita AG, Geissen, Germany) with a maximum rating of 32.5 MPa and a 3 l h^{-1} flow rate *via* jacketed 1/8-inch (SS316) high pressure tubing (Autoclave Engineers).

A polyscience cryostat Model 9505 was used to keep the entire system, autoclave, transfer lines and infrared cell, isothermal. Temperatures were measured at the cryostat, autoclave and IR cell with PT-100 thermoresisters. The necessary connections to vacuum and gases were made with 1/4 inch (SS316) high-pressure tubing (Autoclave Engineers) and 30 MPa manometers were used for pressure measurements (Keller AG, Winter, Switzerland). The entire system is gas-tight under vacuum as well as at 20.0 MPa.

The high-pressure infrared cell was constructed at ETH-Zurich using SS316 steel and could be heated and cooled. The CaF_2 single crystal windows (Korth Monokristalle, Kiel, Germany) have dimensions of 40 mm diameter by 15 mm thickness. Two sets of Viton and silicone gaskets provide the necessary sealing, and Teflon spacers are used between the windows.[74] This high-pressure infrared cell is situated in a Perkin-Elmer SPECTRUM 2000 FT-IR spectrometer. The spectral resolution used in this study was 1 cm^{-1} at an interval of 0.2 cm^{-1} for the range 1000–2500 cm^{-1}. A schematic diagram of the experimental setup can be found in ref .75

In situ spectroscopic studies

As mentioned earlier, the experimental study consisted of seven isothermal semibatch reactions, five under CO and two under helium gas. All of these semibatches were conducted in a similar manner. Thus, only the detailed description of the first isothermal batch, temperature 288 K under CO, is shown in Table 4. The total mass of $[Rh_4(CO)_{12}]$ present in any semibatch experiment was 32–102 mg.

Each of the seven semibatches was initiated as follows. First, background spectra of the IR sample chamber were recorded. Then 100 ml n-hexane was transferred under argon to the autoclave. Under 0.5 MPa of gas, CO or He, infrared spectra of the n-hexane in the high-pressure cell were recorded. The total system pressure was raised to 1.0 MPa, and the stirrer and high-pressure membrane pump were started. After equilibration, infrared spectra of the gas/n-hexane solution in the high-pressure cell were recorded.

At the end of the initial steps, a solution of *ca.* 50 mg $[Rh_4(CO)_{12}]$ dissolved in 50 ml n-hexane was prepared, transferred to the high-pressure reservoir under argon, pressurized and then added to the autoclave. After equilibration, infrared spectra of the $[Rh_4(CO)_{12}]$/dissolved gas/n-hexane solution in the high-pressure cell were recorded.

Each semibatch reaction consisted of six perturbations and the duration of each perturbation was *ca.* two hours. (I) The gas pressure was raised to 1.5 and then (II) to 2 MPa. (III) An additional solution of *ca.* 50 mg $[Rh_4(CO)_{12}]$ dissolved in 50 ml n-hexane was added to the autoclave. The pressure was then raised to (IV) 3.0, (V) 5.0 and (VI) 7.0 MPa CO.

Spectra were recorded at 10 min intervals in the range 1000–2500 cm^{-1}. Each semibatch lasted 14 hours and *ca.* 70 spectra were collected. For the five CO semibatches, temperatures were 288 K, 283 K, 278 K, 273 K and 268 K. A total of 337 spectra were collected. The additional two helium semibatches were performed at temperatures of 293 K and 275 K and 138 spectra were collected.

Table 4 Experiment design using CO at 288 K

CO/MPa	1.0	1.5	2.0	2.0	3.0	5.0	7.0
$Rh_4(CO)_{12}$/mg	52.5	52.5	52.5	96.5	96.5	96.5	96.5
Hexane/ml	200	200	200	250	250	250	250

Acknowledgements

We would like to thank Prof. Brian Heaton (Liverpool, UK) and Prof. John Shapley (University of Illinois, USA) for discussions and Prof. Brian Johnson (Cambridge University, UK) for correspondence. We also would like to thank Assoc. Prof. Fan Wai Yip and Chong Thiam Seong at the Department of Chemistry at NUS for providing the IR spectra of $Ir_4(CO)_{12}$.

References

1 F. A. Cotton, *Inorg. Chem.*, 1966, **5**, 1083.
2 F. A. Cotton, L. Kruczynski, J. Lewis, B. L. Shapiro and L. F. Johnson, *J. Am. Chem. Soc.*, 1972, **94**, 6191.
3 J. Evans, B. F. G. Johnson, J. Lewis, J. R. Norton and F. A. Cotton, *J. Chem. Soc., Chem. Commun.*, 1973, 807.
4 E. Band and E. L. Muetterties, *Chem. Rev.*, 1978, **78**, 636.
5 Y. V. Roberts, B. F. Johnson and R. E. Benfield, *Inorg. Chim. Acta.*, 1995, **229**, 221.
6 T. Eguchi and B. Heaton, *J. Chem. Soc., Dalton Trans.*, 1999, 3523.
7 F. A. Cotton, *Inorg. Chem.*, 2002, **41**, 643.
8 D. L. Kepert and S. C. Williams, *J. Organomet. Chem.*, 1981, **217**, 235.
9 B. F. G. Johnson, *J. Chem. Soc., Chem. Commun.*, 1976, 211.
10 J. Evans, B. F. G. Johnson, J. Lewis, T. E. Matheson and J. R. Norton, *J. Chem. Soc., Dalton Trans.*, 1978, 626.
11 P. Corradini, *J. Chem. Phys.*, 1959, **31**, 1676.
12 P. Corradini and A. Sirigu, *Ric. Sci.*, 1966, **36**, 188.
13 C. H. Wei and L. F. Dahl, *J. Am. Chem. Soc.*, 1966, **88**, 1821.
14 C. H. Wei, *Inorg. Chem.*, 1969, **8**, 2384.
15 F. H. Carre, F. A. Cotton and B. A. Frenz, *Inorg. Chem.*, 1976, **15**, 380.
16 L. J. Farrugia, D. Braga and F. Grepioni, *J. Organomet. Chem.*, 1999, **573**, 60.
17 G. Bor, *Spectrochim. Acta*, 1963, **19**, 1209.
18 G. Bor, G. Sbrignadello and K. Noak, *Helv. Chim. Acta*, 1975, **58**, 815.
19 S. Aime, R. Gobetto, D. Osella, L. Milone, G. E. Hawkes and E. W. Randall, *J. Magn. Reson.*, 1985, **65**, 308.
20 S. Aime, D. Osella, L. Milone, G. E. Hawkes and E. W. Randal, *J. Am. Chem. Soc.*, 1981, **103**, 5920.
21 E. A. C. Lucken, K. Noack and D. F. Williams, *J. Chem. Soc. A*, 1967, 148.
22 H. Haas and R. K. Sheline, *J. Inorg. Nucl. Chem.*, 1967, **29**, 693.
23 M. A. Cohen, D. R. Kidd and T. L. Brown, *J. Am. Chem. Soc.*, 1975, **97**, 4408.
24 S. Aime, L. Milone, D. Osella and A. Poli, *Inorg. Chim. Acta*, 1978, **30**, 45.
25 J. Evans, B. F. G. Johnson, J. Lewis and T. W. Matheson, *J. Am. Chem. Soc.*, 1975, **97**, 1245.
26 S. Aime and L. Milone, *Prog. Nucl. Magn. Reson. Spectrosc.*, 1977, **11**, 183.
27 M. R. Churchill and J. P. Hutchinson, *J. Inorg. Chem.*, 1978, **12**, 3528.
28 G. R. Wilkes, Ph.D. Thesis, University of Wisconsin, Madison, WI, 1965.
29 G. F. Stuntz, Ph. D. Thesis, University of Illinois, Urbana-Champaign, IL, 1978.
30 F. Cariati, V. Valenti and G. Zerbi, *Inorg. Chim. Acta*, 1969, **3**, 378.
31 W. Heiber and H. Legally, *Z. Anorg. Allg. Chem.*, 1943, **96**, 251.
32 P. Chini and S. Martinengo, *Chem. Commun.*, 1968, **5**, 251.
33 P. Chini and S. Martinengo, *Inorg. Chim. Acta*, 1969, **3**, 315.
34 P. Chini and B. T. Heaton, *Top. Curr. Chem.*, 1977, **71**, 1.
35 C. H. Wei, G. R. Wilkes and L. F. Dahl, *J. Am. Chem. Soc.*, 1967, **89**, 4792.
36 L. J. Farrugia, *J. Cluster Sci.*, 2000, **11**, 39.
37 J. A. Creighton and B. T. Heaton, *J. Chem. Soc., Dalton Trans.*, 1981, 1972.
38 B. T. Heaton, L. Strona, R. Della Pergola, L. Garlaschelli, U. Sartorelli and I. H. Sadler, *J. Chem. Soc., Dalton Trans.*, 1983, 173.
39 L. M. Jackman and F. A. Cotton, *Dynamic Nuclear Magnetic Resonance*, Academic Press, New York, NY, 1975.
40 R. E. Benfield and B. F. G. Johnson, *J. Chem. Soc., Dalton Trans.*, 1978, 1554.
41 J. W. Lauher, *J. Am. Chem. Soc.*, 1986, **108**, 1521.
42 R. Whyman, *J. Chem. Soc., Dalton Trans.*, 1972, 1375.

43 F. Oldani and G. Bor, *J. Organomet. Chem.*, 1983, **246**, 309.
44 J. Vidal and W. E. Walker, *Inorg. Chem.*, 1981, **20**, 249.
45 G. A. Ozin and A. J. Hanlan, *Inorg. Chem.*, 1979, **18**, 2091.
46 A. J. Hanlan and G. A. Ozin, *J. Am. Chem. Soc.*, 1974, **20**, 6324.
47 B. T. Heaton and L. Longhetti, *J. Organomet. Chem.*, 1981, **213**, 333.
48 P. J. Chini, *Chem. Commun.*, 1967, 440.
49 W. A. Weber and B. C. Gates, *J. Phys. Chem. B*, 1997, **101**, 10423.
50 W. Chew, E. Widjaja and M. Garland, *Organometallics*, 2002, **21**, 1882.
51 E. Widjaja, C. Li and M. Garland, *Organometallics*, 2002, **21**, 1991.
52 C. Li, E. Widjaja, W. Chew and M. Garland, *Angew. Chem., Int. Ed.*, 2002, **20**, 3785.
53 G. Bouquet and M. Bigorna, *Spectrochim. Acta, Part A*, 1971, **27**, 139.
54 M. Bigorna, *J. Organomet. Chem.*, 1970, **24**, 211.
55 W. Chew, E. Widjaja and M. Garland, *Organometallics*, 2002, **21**, 1982.
56 W. Beck and K. Lottes, *Chem. Ber.*, 1961, **94**, 2578.
57 E. R. Corey and L. F. Dahl, *J. Am. Chem. Soc.*, 1963, **85**, 1203.
58 E. Widjaja, C. Li and M. Garland, *J. Catal.*, 2004, **223**, 278.
59 M. Garland and P. Pino, *Organometallics*, 1991, **10**, 1693.
60 K. S. Suslick, E. B. Flint and J. A. Jensen, *J. Chem. Educ.*, 1987, **64**, 547.
61 J. C. Owrutsky and A. P. Barnovski, *J. Chem. Phys.*, 1996, **105**, 9864.
62 P. S. Braterman, *Metal Carbonyl Spectra*, Academic Press, London, 1975, pp. 153–15.
63 L. J. Farrugia, *J. Chem. Soc., Dalton Trans.*, 1997, 1783.
64 A. McCellan, *Tables of Experimental Dipole Moments*, W. H. Freeman, San Francisco, CA, 1963, vol. 1, pp. 28, 220.
65 J. M. Prausnitz, R. N. Lichtenthaler and E. G. Azevedo, *Molecular Thermodynamics of Fluid-Phase Equilibria*, Prentice Hall, New Jersey, 3rd edn., 1999, p. 62.
66 D. T. Brown, T. E. Eguchi, B. T. Heaton, J. A. Iggo and R. Whyman, *J. Chem. Soc., Dalton Trans.*, 1991, 677.
67 K. Noack, *Spectrochim. Acta*, 1963, **19**, 1925.
68 K. Noack, *Helv. Chim. Acta*, 1964, **47**, 1064.
69 R. L. Sweany and T. L. Brown, *Inorg. Chem.*, 1977, **16**, 415.
70 M. Garland and G. Bor, *Inorg. Chem.*, 1989, **28**, 410.
71 D. V. Krupenya, E. O. Danilov, M. A. J. Rodgers and S. P. Tunik, *J. Phys. Chem. A*, 2003, **107**, 8867.
72 G. Bor, U. K. Dietler and P. Pino, *J. Organomet. Chem.*, 1978, **154**, 301.
73 D. F. Shriver and M. A. Drezdzon, *The Manipulation of Air-Sensitive Compounds*, Wiley, New York, 1986.
74 R. Whyman, in *Laboratory Methods in Vibrational Spectroscopy*, ed. H. A. Willis, J. H. van der Maas and R. G. J. Miller, Wiley, New York, 3rd edn., 1987, ch. 12.
75 J. Feng and M. Garland, *Organometallics*, 1999, **18**, 417.